CENTER FOR INFRASTRUCTURE ENGINEERING STUDIES

Modeling of Composite Hydrogen Storage Cylinders Using Finite Element Analysis

by

K. Chandrashekhara

A University Transportation Center Program at Missouri University of Science & Technology

Disclaimer

The contents of this report reflect the views of the author(s), who are responsible for the facts and the accuracy of information presented herein. This document is disseminated under the sponsorship of the Department of Transportation, University Transportation Centers Program and the Center for Infrastructure Engineering Studies UTC program at the University of Missouri - Rolla, in the interest of information exchange. The U.S. Government and Center for Infrastructure Engineering Studies assumes no liability for the contents or use thereof.

Technical Report Documentation Page

1. Report No.	2. Government Accession No.	3. Recipient's Catalog No.
UTC R170		

4. Title and Subtitle	5. Report Date
Modeling of Composite Hydrogen Storage Cylinders Using Finite Element Analysis	February 2008
	6. Performing Organization Code

7. Author/s	8. Performing Organization Report No.
K. Chandrashekhara	00013052

9. Performing Organization Name and Address	10. Work Unit No. (TRAIS)
Center for Infrastructure Engineering Studies/UTC program Missouri University of Science & Technology 223 Engineering Research Lab Rolla, MO 65409	11. Contract or Grant No. DTRS98-G-0021

12. Sponsoring Organization Name and Address	13. Type of Report and Period Covered
U.S. Department of Transportation Research and Special Programs Administration 400 7th Street, SW Washington, DC 20590-0001	Final
	14. Sponsoring Agency Code

15. Supplementary Notes

16. Abstract

Pressurized hydrogen storage cylinders are critical components of hydrogen transportation systems. Composite cylinders have pressure/thermal relief devices that are activated in case of an emergency. The difficulty in accurately analyzing the behavior of a filament wound composite storage cylinder derives from continually varying orientation of the fibers. In the proposed research, a finite element model will be developed to perform thermo-mechanical analysis of storage cylinders. Optimization of design variables such as, cylinder size, type of liner, fiber orientation, thickness of the various layers, and location of the pressure relief device will be performed.

17. Key Words	18. Distribution Statement
Hydrogen storage cylinder, finite element analysis, pressure/thermal relief devices	No restrictions. This document is available to the public through the National Technical Information Service, Springfield, Virginia 22161.

19. Security Classification (of this report)	20. Security Classification (of this page)	21. No. Of Pages	22. Price
unclassified	unclassified	13	

Form DOT F 1700.7 (8-72)

FINAL REPORT
UMR - UNIVERSITY TRANSPORTATION CENTER
ADVANCED MATERIALS AND NON-DESTRUCTIVE TESTING TECHNOLOGIES

Sequential #: R170

Project Title: UTC/Transportation Fuel Research and Development-Modeling of Composite Hydrogen Storage Cylinders Using Finite Element Analysis

Principal Investigator: K. Chandrashekhara, Professor, Department of Mechanical and Aerospace Engineering

Project Duration: 5/1/06-12/31/06

Amount: Not shown

Project Summary:

Safe installation and operation of lightweight composite hydrogen storage cylinders are of primary concern. Typically, the inner liner of the cylinder is made with a high molecular weight polymer or aluminum that serves as a hydrogen gas permeation barrier. A filament-wound, carbon/epoxy composite laminate placed over the liner provides the desired pressure load bearing capacity. In many current designs, a glass/epoxy layer or other material is placed over the carbon/epoxy laminate to provide impact and damage resistance. These cylinders also have pressure/thermal relief devices that are activated in case of an emergency. The difficulty in accurately analyzing the behavior of a filament wound composite storage cylinder derives form the continually varying orientation of the fibers. Most of the analysis reported in filament wound composite cylinders is based on simplifying assumptions and does not account for complexities like thermo-mechanical behavior and highly orthotropic nature of the material. In the present work, a comprehensive finite element simulation tool for the design of hydrogen storage cylinder system is developed. The structural response of the cylinder is analyzed using laminated shell theory accounting for transverse shear deformation and geometric nonlinearity. A composite failure model is used to predict the maximum burst pressure. Results for various thermo-mechanical loading cases are presented.

Introduction:

Composite high-pressure cylinders (CHC's) have potential application as hydrogen storage systems in automotives and transportation systems due to their light weight, simplicity of the storage and low cost for storage and transport of hydrogen gas. Typically, a composite high-pressure cylinder is made with a high molecular weight polymer or aluminum liner that serves as a hydrogen gas permeation barrier. A filament-wound, carbon/epoxy composite laminate over-wrapped outside of the liner provides the desired pressure load bearing capacity. The cylinder is capable of sustaining pressures of

5000 psi or higher by taking advantage of high modulus, high strength and low specific weight of modern high performance composite. In addition, the maturation of filament winding manufacturing process further lowers the price to practical and common usage in mass transportation systems.

To design composite high-pressure cylinders with the most possible safety, reliability and minimum weight considerations, the behavior of composite structures under various mechanical and thermal loadings need to be well understood. Compared to pure mechanical loading, fewer studies have been conducted on CHC's subjected to thermal loads and combined thermo-mechanical loads. In the present study, a thermo-mechanical finite element model has been developed for the analysis of hydrogen storage cylinders. The composite lamina wrap of hydrogen CHC typically consists of helical laminated layers and hoop laminated layers. Both these layers along with an aluminum liner are considered for the analysis (Figure 1). During service, hydrogen CHC's unavoidably experience various thermal loadings combined with high pressure. To account for environmental temperature variation, uniform temperature loadings ranging from 25°C to 140° C are considered for the analysis. During the gas filling process, the inner temperature can increase to around 100 °C. Hence, non-uniform thermal loadings have also been considered. The variation of material properties with temperature is significant for most composites. A temperature dependent material model has been developed and implemented in commercial finite element code ABAQUS, using user subroutines. A laminated shell theory accounting for out-of-plane shear strains and geometric nonlinearity is used for the analysis.

Shear Deformable Shell Theory:

The major loading bearing component of hydrogen storage cylinders is the carbon/epoxy composite shell wrapped around the cylinder liner (shown in Figure 2). The composite shell experiences not only in-plane deformation but also out-of-plane shear strains. The doubly curved shell theory accounting for out of plane shear deformations and geometric nonlinearity is used for the analysis of composite hydrogen storage cylinders.

A multilayered doubly curved shell is shown in Figure 3. The curved coordinated system $\{\xi_1, \ \xi_2, \ \zeta\}$ is used in space description. The coordinates ξ_1 and ξ_2 specify the position on the middle surface, while ζ measures the distance, along the outward normal, from the mid-surface to arbitrary point on the shell. The displacement field can be written as:

$$u(\xi_1, \xi_2, \zeta) = (1 + \frac{\zeta}{R_1})\, u_o(\xi_1, \xi_2) + \zeta\, \phi_1(\xi_1, \xi_2) \tag{1.a}$$

$$v(\xi_1, \xi_2, \zeta) = (1 + \frac{\zeta}{R_2})\, v_o(\xi_1, \xi_2) + \zeta\, \phi_2(\xi_1, \xi_2) \tag{1.b}$$

$$w(\xi_1, \xi_2, \zeta) = w_o(\xi_1, \xi_2) \tag{1.c}$$

The non-linear strain-displacement relations based on Sanders's shell theory can be given as:

$$\varepsilon_x = \varepsilon_x^o + \zeta\,\kappa_x \;;\quad \varepsilon_y = \varepsilon_y^o + \zeta\,\kappa_y$$
$$\gamma_{xy} = \gamma_{xy}^o + \zeta\,\kappa_{xy} \;;\quad \gamma_{yz} = \gamma_{yz}^o \;;\quad \gamma_{xz} = \gamma_{xz}^o \tag{2}$$

where ε_j^0 and κ_j are defined as:

$$\varepsilon_x^o = \frac{1}{\alpha_1}\frac{\partial u_o}{\partial \xi_1} + \frac{w_o}{R_1} + \frac{1}{2\alpha_1^2}\left(\frac{\partial w_o}{\partial \xi_1}\right)^2 \;;\; \kappa_x = \frac{1}{\alpha_1}\frac{\partial \phi_1}{\partial \xi_1}$$
$$\varepsilon_y^o = \frac{1}{\alpha_2}\frac{\partial v_0}{\partial \xi_2} + \frac{w_0}{R_2} + \frac{1}{2\alpha_2^2}\left(\frac{\partial w_o}{\partial \xi_2}\right)^2 \;;\; \kappa_y = \frac{1}{\alpha_2}\frac{\partial \phi_2}{\partial \xi_2}$$
$$\gamma_{xy}^o = \frac{1}{\alpha_1}\frac{\partial v_o}{\partial \xi_1} + \frac{1}{\alpha_2}\frac{\partial u_o}{\partial \xi_2} + \frac{1}{2\alpha_1\alpha_2}\frac{\partial w_o}{\partial \xi_1}\frac{\partial w_o}{\partial \xi_2} \;;\; \gamma_{yz}^o = \frac{1}{\alpha_2}\frac{\partial w_o}{\partial \xi_2} + \phi_2 - \frac{v_o}{R_2} \tag{3}$$
$$\gamma_{xz}^o = \frac{1}{\alpha_1}\frac{\partial w_o}{\partial \xi_1} + \phi_1 - \frac{u_o}{R_1}$$
$$\kappa_{xy} = \frac{1}{\alpha_1}\frac{\partial \phi_2}{\partial \xi_1} + \frac{1}{\alpha_2}\frac{\partial \phi_1}{\partial \xi_2} - c_o\left(\frac{1}{\alpha_1}\frac{\partial v_o}{\partial \xi_1} - \frac{1}{\alpha_2}\frac{\partial u_o}{\partial \xi_2}\right)$$
$$c_0 = \frac{1}{2}\left(\frac{1}{R_1} - \frac{1}{R_2}\right);\; dx = \alpha_1 d\xi_1;\; dy = \alpha_2 d\xi_2$$

In Eq. (3), u and v are the displacements in the direction of the tangents to the coordinate lines ξ_1 and ξ_2, respectively, w is the displacement in the direction of the outward normal and ϕ_1 and ϕ_2 are the rotations.

The stress-strain relation, accounting for thermal effects, in the shell coordinates for a k^{th} layer can be expressed as:

$$\begin{Bmatrix} \sigma_x \\ \sigma_y \\ \tau_{xy} \\ \tau_{yz} \\ \tau_{xz} \end{Bmatrix}_k = \begin{bmatrix} Q_{11} & Q_{12} & Q_{16} & 0 & 0 \\ Q_{12} & Q_{22} & Q_{26} & 0 & 0 \\ Q_{16} & Q_{26} & Q_{66} & 0 & 0 \\ 0 & 0 & 0 & Q_{44} & Q_{45} \\ 0 & 0 & 0 & Q_{45} & Q_{55} \end{bmatrix}_k \begin{Bmatrix} \varepsilon_x - \alpha_x T \\ \varepsilon_y - \alpha_y T \\ \gamma_{xy} - \alpha_{xy} T \\ \gamma_{yz} \\ \gamma_{xz} \end{Bmatrix}_k \tag{4}$$

where Q_{ij} are the transformed elastic coefficients, T is the given temperature distribution, $(\alpha_x, \alpha_y, \alpha_{xy})$ are the thermal expansion coefficients in the shell coordinates.

The laminate constitutive equations can be obtained by integrating Eq. (4) over the thickness, and is written as:

$$\begin{Bmatrix} N_x \\ N_y \\ N_{xy} \\ Q_{xz} \\ Q_{yz} \\ M_x \\ M_y \\ M_{xy} \end{Bmatrix} = \begin{bmatrix} A_{11} & A_{12} & A_{16} & 0 & 0 & B_{11} & B_{12} & B_{16} \\ A_{12} & A_{22} & A_{26} & 0 & 0 & B_{12} & B_{22} & B_{26} \\ A_{16} & A_{26} & A_{66} & 0 & 0 & B_{16} & B_{26} & B_{66} \\ 0 & 0 & 0 & A_{44} & A_{45} & 0 & 0 & 0 \\ 0 & 0 & 0 & A_{45} & A_{55} & 0 & 0 & 0 \\ B_{11} & B_{12} & B_{16} & 0 & 0 & D_{11} & D_{12} & D_{16} \\ B_{12} & B_{22} & B_{26} & 0 & 0 & D_{12} & D_{22} & D_{26} \\ B_{16} & B_{26} & B_{66} & 0 & 0 & D_{16} & D_{26} & D_{66} \end{bmatrix} \begin{Bmatrix} \varepsilon_x^0 \\ \varepsilon_y^0 \\ \gamma_{xy}^0 \\ \gamma_{xz}^0 \\ \gamma_{yz}^0 \\ \kappa_x \\ \kappa_y \\ \kappa_{xy} \end{Bmatrix} - \begin{Bmatrix} N_x^T \\ N_y^T \\ N_{xy}^T \\ 0 \\ 0 \\ M_x^T \\ M_y^T \\ M_{xy}^T \end{Bmatrix} \tag{5}$$

where N^T and M^T are thermal stress and moment resultants

$$\left(A_{ij} \quad B_{ij} \quad D_{ij}\right) = \int_{-h/2}^{h/2} Q_{ij} \left(1 \quad z \quad z^2\right) dz \ \left(i, j = 1, 2, 6\right) \tag{6.a}$$

$$A_{ij} = \int_{-h/2}^{h/2} K_i K_j Q_{ij} dz \ \left(i, j = 4, 5\right) \tag{6.b}$$

$$\begin{Bmatrix} N_x^T, & M_x^T \\ N_y^T, & M_y^T \\ N_{xy}^T, & M_{xy}^T \end{Bmatrix} = \int_{-h/2}^{h/2} \begin{bmatrix} Q_{11} & Q_{12} & Q_{16} \\ Q_{12} & Q_{22} & Q_{26} \\ Q_{16} & Q_{26} & Q_{66} \end{bmatrix} \begin{Bmatrix} \alpha_x \\ \alpha_y \\ \alpha_{xy} \end{Bmatrix} \left(1, \quad z\right) T dz \tag{6.c}$$

where K is shear correction factor.

Following the standard finite element procedure, the generalized displacements in any element are given by

$$\begin{Bmatrix} u \\ v \\ w \\ \phi_1 \\ \phi_2 \end{Bmatrix} = \sum_{i=1}^{N} \begin{Bmatrix} u \\ v \\ w \\ \phi_1 \\ \phi_2 \end{Bmatrix}_i \psi_i \tag{7}$$

where N is the number of nodes in the element and ψ_i are the interpolation functions.

Substituting Eq. (7) in Eq. (3), the strains can be expressed as

$$\varepsilon = B_1 \Delta \ ; \quad \kappa = B_2 \Delta \ ; \quad \gamma = B_3 \Delta \tag{8}$$

The finite element equation is written as

$$\left[K^e\right]\left\{\Delta^e\right\} = \left\{F^e\right\} + \left\{F_T^e\right\} \tag{9}$$

where

$$\left[K^e\right] = \iint \left(B_1^T A B_1 + B_1^T B B_2 + B_2^T B B_1 + B_2^T D B_2 + B_3^T S B_3\right) d(Area)$$

$$\left\{\Delta^e\right\} = \left\{\{u\} \quad \{v\} \quad \{w\} \quad \{\phi_1\} \quad \{\phi_2\}\right\}^T$$

$$\left\{F^e\right\} = \iint \left(B_1^T N \ + B_2^T M \ \right) \cdot d(Area)$$

$$\left\{F_T^e\right\} = \iint \left(B_1^T N^T + B_2^T M^T\right) \cdot d(Area)$$

For any given mechanical and temperature loadings, Eq. (9) can be assembled and solved to determine displacements and stresses.

Composite Failure Model:

Failure in composites is a complicated phenomenon and usually involves processes such as fiber break, matrix cracking, de-bonding of the fiber and matrix, and fiber bulking. In order to relate these failure modes to some evaluable physical quantities (stress, strain or energy), a considerable number of failure theories for composite have been proposed. However, only the most common and well tested theories are applicable in failure prediction. Tsai-Wu failure theory is a simplification of Gol'denblat and Kapnov's generalized failure theory for anisotropic materials. It was originally developed to predict the failure of filamentary composite materials and experimentally verified by many authors. Tsai-Wu failure criterion is used here for composite failure evaluation. Taking 1 as fiber direction and 2 and 3 as transverse directions, the Tsai-Wu failure criterion can be expressed as:

$$\begin{aligned} I_F = {} & F_1\sigma_{11} + F_2\sigma_{22} + F_{11}\sigma_{11}^2 + F_{22}\sigma_{22}^2 + F_{44}\sigma_{23}^2 \\ & + F_{55}\sigma_{13}^2 + F_{66}\sigma_{12}^2 + 2F_{12}\sigma_{11}\sigma_{22} \ < 1.0 \end{aligned} \tag{10}$$

The coefficients in Eq. (10) are defined as:

$$F_1 = \frac{1}{X_t} + \frac{1}{X_c}, \ F_2 = \frac{1}{Y_t} + \frac{1}{Y_c}, F_{11} = -\frac{1}{X_t X_c},$$

$$F_{22} = -\frac{1}{Y_t Y_c}, F_{44} = \frac{1}{S_{23}^2}, F_{55} = \frac{1}{S_{13}^2}, F_{66} = \frac{1}{S_{12}^2},$$

$$F_{12} = \frac{1}{2\sigma_{biax}^2}\left[1 - \left(\frac{1}{X_t} + \frac{1}{X_c} + \frac{1}{Y_t} + \frac{1}{Y_c}\right)\sigma_{biax} + \left(\frac{1}{X_t X_c} + \frac{1}{Y_t Y_c}\right)\sigma_{biax}^2\right]$$

or

$$F_{12} = f\sqrt{F_{11}F_{22}} \quad (-1 \le f \le 1)$$

where, X_t and X_c are tensile and compressive stress strength along fiber direction, Y_t and Y_c are tensile and compressive stress strength in transverse fiber direction, S_{23}, S_{13} and S_{12} are the maximum shear strength in corresponding planes, σ_{biax} is the equi-biaxial stress at failure and f is an experience coefficient.

Material Properties:

Carbon fiber reinforced composites are widely used as structural materials in lightweight hydrogen storage because of their high specific strengths, moduli, and design flexibilities. However, mechanical and thermal properties of fiber reinforced composites vary significantly with temperature. As the carbon/epoxy laminate carries the pressure loading from the hydrogen gas, the effect of temperature on its material properties can not be ignored. The moduli and thermal expansion coefficients are dependent on temperature. For HFG CU125 carbon/epoxy, the temperature dependent material properties and are given by:

$$\begin{gathered} E_1 = -0.66\,T + 128\ (\text{GPa})\ (25°C < T < 140°C) \\ E_2 = -0.064\,T + 10.67\ (\text{GPa})\ (25°C < T < 140°C) \\ G_{12} = 0.034\,T + 5.39\ (\text{GPa})\ (25°C < T < 140°C) \\ \upsilon_{12} = -0.0005\,T + 0.44\ (25°C < T < 140°C) \\ \alpha_1 = (0.0003\ T^2 - 0.04\ T + 2.09) \times 10^{-6}\ (30°C < T < 130°C) \\ \alpha_2 = (0.0041\ T^2 - 0.23\ T + 32.2) \times 10^{-6}\ (30°C < T < 130°C) \end{gathered} \tag{11}$$

Furthermore, G_{13} is taken as G_{12} and G_{23} is assumed as 0.7 G_{12}. The ultimate strengths of carbon/epoxy do not change much with temperature and are assumed to be constant and are listed in Table 1. The material properties for glass/epoxy are listed in Table 2. The outer most glass/epoxy layer is only used for protection of the load bearing carbon/epoxy lamina. Hence temperature dependent material properties are not used for the glass/epoxy layers. Properties of innermost aluminum liner are listed in Table 3.

Numerical Simulation:

The storage cylinder considered for the analysis has an inner diameter R_{in} = 0.44 m and outer diameter R_{out} = 0.47 m (Figure 3). The wall consists of innermost liner, carbon/epoxy laminate (helical and hoop) and an outermost protection glass/epoxy layer. The thickness of the liner is 2.5 mm. The helical and hoop laminates have a total thickness of 28 mm and protective glass/epoxy layer is 2 mm thick.

In the present work, the total thickness of helical and hoop laminates do not change, but the thickness ratio (thickness of helical laminates over hoop laminates) varies. The optimized thickness ratio can be obtained by identifying the maximum burst pressure while thickness ratio varies in a range of 0.1 to 2.0. With the combined consideration of manufacturing capability and the possible higher burst pressure, the winding angle (the angle between fiber and axial direction or direction 3 in helical layer) usually fall in a span ranging from 10° to 30°. To cover this range, three cases with different winding angles 10°, 20° and 30° respectively are considered in this study. The lay up of helical lamina is chosen as $[\theta^\circ/-\theta^\circ]_{6s}$ (θ=10°, 20° and 30°). In hoop layer, fiber direction is ideally supposed to be 90°. The lamina is oriented as $[89^\circ/-89^\circ]_{6s}$ for manufacturing possibility. The fiber direction in protection layer is taken as [45°/-45°] cross ply. For each case, the temperatures for uniform thermal loading are taken as 25°C, 50°C, 75°C, 100°C, 120°C

and 140°C. For non-uniform temperature loading, the temperature distribution varies linearly across the thickness (inner to outer) from 25°C to 140°C, 50°C to 120°C, and 75°C to 100°C and inverse.

ABAQUS is a reliable finite element code for solving general solid mechanics, heat transfer and fluid problems. It is widely used by the industry as well as researchers for its flexibility of implementing user defined subroutine and its powerful nonlinear solver. The failure model, the temperature dependent material properties, and fiber orientations are implemented in ABAQUS using user subroutines. Taking advantage of symmetry, only $1/8^{th}$ of the hydrogen cylinder is modeled and meshed using ABAQUS/CAE as shown in Figure 4. The composite shell uses the S4R element which is based on a doubly curved shell element accounting for transverse shear deformation. Solid brick element C3D8R is used for liner. The model is solved by using ABAQUS/standard solver. The results obtained of each case are listed in Tables 4 through 6 and selected results are plotted and discussed.

Results and Discussion:

Three different winding orientations of the helical layers 10°, 20° and 30° have been considered for the analysis. Also, uniform temperature distribution (cylinder inner temperature = cylinder outer temperature), and a variety temperature gradients (cylinder inner temperature < outer temperature, cylinder inner temperature > outer temperature) have also been considered for the analysis. Burst pressures as a function of thickness ratio for these temperature distributions are presented.

Figures 5, 6 and 7 plot the variation of burst pressure as a function of thickness ratio (total thickness of helical laminates/total thickness of hoop laminates) for various uniform temperature distributions. It can be seen that with increasing temperature the burst pressure goes up in each case under uniform thermal loading. In non-uniform thermal loading cases (Figures 8 through 13), the burst pressure drops dramatically with increasing temperature. This may be explained by observing the failure pattern plotted in Figures 14 and 15 for Case 2 (winding angle = 20°). Figures 14 and 15 plot the failure coefficients as a function of the layer number for a thickness ratio of 0.75. In Figure 14, it can be seen that with increasing temperature, the failure coefficient of layers (based on Tsai-Wu failure) are close together, which means the load is more evenly distributed in each layer. This even load distribution contributes to the significant increase in burst pressure. For non-uniform thermal loading cases (Figure 15), the failure coefficients for the various layers are not close together and have a slope indicating that the applied load is not evenly distributed among the layers (some layers have high stress as compared to others causing them to fail first). This explains the dramatic drop in burst pressure when non-uniform temperature field in applied.

When the cylinder is experiencing uniform thermal loading (Figures 5, 6 and 7), there is a peak pressure which can be found in each case. The thickness ratio at the peak pressure is approximately 0.5 when the winding angle is 10° and 0.75 in when the winding angle is 20° and 30°. With increasing winding angle, marginal effect of optimized thickness ratio

becomes more obvious. The curve around the peak pressure becomes flatter and the optimized thickness ratio is over a wider range. Also, under non-uniform thermal loading when the inner temperature is lower (Figures 8 through 10) the optimized thickness ratio shifts much to the left side. For non-uniform temperature distribution, when the inner temperature is higher, there is no obvious peak pressure (Figures 11 through 13). Axial loading is mainly sustained by the helical layers. When the inner temperature is higher, the axial loading is transferred to the hoop layers because of the higher thermal expansion of the helical layers. However, the hoop layers cannot sustain axial loading (as the reinforcement is not along the direction of the load) and hence a distinct peak does no occur in the curve.

For non uniform thermal loading, when the inner temperature is lower, it can be seen that the failure coefficient is higher in the inner layers (Figure 15). Hence, when the inner temperature is lower, the inner layers fail first. When the inner temperature is higher, the outer layers fail first as the inner thermal strain is higher than the strain in the outer layers. The outer layers sustain the majority of mechanical loading causing them to fail first. This is also reflected in Figure 15 with outer layers having higher failure coefficients.

Conclusions:

A doubly curved shell model that is capable of treating both thick and thin cylindrical shells with thermal loading is used for the finite element simulation of composite high pressure storage cylinders. Temperature dependent material properties of the load carrying carbon/epoxy layer and geometry nonlinearity are also considered in the numerical model. Three typical cases have been considered and the analysis is carried out by applying uniform/non-uniform thermal loading and high pressure mechanical loading. Tsai-Wu failure criterion is employed to predict the burst pressure by checking the failure layer by layer. Under uniform thermal loading, a temperature increase significantly increases maximum burst pressure. Contrastively, the non-uniform thermal loading can cause an uneven load distribution and hence decrease the maximum burst pressure. The ratio of thickness of the helical layer to the hoop layer also plays an important role in determining the maximum burst pressure and should be selected appropriately based on the thermal and mechanical loading conditions.

Acknowledgements:

The project is sponsored by the US. Department of Transportation and University Transportation Center.

Publication:

1. S. Sundararaman, J. Hu, K. Chandrashekhara and W. Chernicoff, “Thermomechanical Analysis of Composite Cylinders for Hydrogen Storage,” Proceedings of the SAMPE Conference, Baltimore, MD, June 3-7, 2006 (To appear).

Table 1. Ultimate strength of carbon/epoxy composite

Strength	F_L^t	F_L^c	F_T^t	F_T^c	F_{LT}^S
MPa	1070	1070	40	170	70

Table 2. Mechanical and thermal properties of S-glass/epoxy

E_1 (GPa)	E_2 (GPa)	$G_{12} = G_{13}$ (GPa)	G_{23} (GPa)	υ_{12}	α_1 (1/°C)	α_2 (1/°C)
55	16	7.6	5.0	0.28	6.3×10^{-6}	32×10^{-6}
Strength	F_L^t	F_L^c	F_T^t	F_T^c	F_{LT}^S	
MPa	1620	690	40	140	60	

Table 3. Mechanical and thermal properties of Aluminum 6061-T6

Elastic Modulus	Poisson's ratio	Yield strength	Thermal expansion
70 GPa	0.33	455 MPa	24.3×10^{-6}

Table 4.a Burst pressure varying with uniform temperature and thickness ratio (Case 1: winding angle 10°)

	Thickness Ratio								
Temp	0.10	0.25	0.50	0.75	1.00	1.25	1.50	1.75	2.00
25	25.80	32.90	36.20	35.00	33.20	31.40	29.80	28.30	27.36
50	27.60	34.80	38.00	36.67	34.87	33.07	31.20	29.90	28.37
75	30.40	37.40	40.50	39.25	37.25	35.50	33.50	32.29	30.88
100	31.20	39.00	42.50	41.50	39.50	37.50	35.50	33.88	32.37
120	32.25	41.00	44.82	44.38	42.38	39.88	37.88	36.71	34.88
140	34.80	45.65	51.30	51.00	48.90	46.50	44.10	43.05	40.65

* Pressure in MPa and temperature in °C

Table 4.b Burst pressure varying with gradient temperature and thickness ratio (Case 1: winding angle 10°)

	Thickness Ratio									Temp.
Temp.	0.10	0.25	0.50	0.75	1.00	1.25	1.50	1.75	2.00	Difference
25-140	22.30	25.20	23.80	21.90	19.90	18.70	17.50	16.30	15.50	115
50-120	25.10	29.40	29.10	27.10	25.50	23.90	22.30	21.10	19.90	70
75-100	29.10	35.80	36.70	35.10	33.10	31.50	29.50	28.30	27.10	25
140-25	16.60	20.00	23.80	25.80	26.60	27.00	26.80	26.70	26.00	115
120-50	20.80	25.40	29.80	31.60	32.00	31.80	31.40	31.10	30.00	70
100-75	27.20	33.40	37.80	38.93	38.70	36.70	34.70	33.10	31.10	25
85-85	30.88	38.38	41.38	40.38	38.38	36.38	34.38	32.88	31.38	0

* Pressure in MPa and temperature in °C

Table 5.a Burst pressure varying with uniform temperature and thickness ratio (Case 2: winding angle 20°)

	Thickness Ratio								
Temp.	0.10	0.25	0.50	0.75	1.00	1.25	1.50	1.75	2.00
25	24.70	31.50	34.30	35.50	34.30	33.10	31.50	29.90	28.70
50	26.70	33.50	35.90	37.50	35.90	34.70	33.10	31.50	30.30
75	29.59	36.34	38.59	39.94	38.59	36.79	35.44	33.64	32.29
100	30.34	37.38	40.88	42.34	40.88	39.38	37.34	35.88	34.34
120	31.21	39.46	43.86	45.51	43.86	42.21	40.56	38.36	36.71
140	33.45	43.65	50.25	51.45	50.25	48.45	46.05	44.25	42.45

* Pressure in MPa and temperature in °C

Table 5.b Burst pressure varying with gradient temperature and thickness ratio (Case 2: winding angle 20°)

	Thickness Ratio									Temp.
Temp.	0.10	0.25	0.50	0.75	1.00	1.25	1.50	1.75	2.00	Difference
25-140	21.50	24.70	24.70	23.10	21.50	19.90	18.70	17.50	16.70	115
50-120	24.70	29.10	29.90	28.30	26.89	25.10	23.74	22.70	21.49	70
75-100	28.30	35.10	37.10	36.30	34.88	33.10	31.38	29.90	28.88	25
140-25	16.30	19.50	23.10	25.50	26.70	27.10	27.10	27.10	27.10	115
120-50	20.30	24.70	29.10	31.10	32.90	32.30	32.20	31.90	31.39	70
100-75	26.70	32.30	37.10	39.10	39.38	38.30	36.34	34.70	33.38	25
85-85	29.88	36.88	41.38	40.34	39.38	37.88	35.88	34.38	32.88	0

* Pressure in MPa and temperature in °C

Table 6.a Burst pressure varying with uniform temperature and thickness ratio (Case 3: winding angle 30°)

	Thickness Ratio								
Temp.	0.10	0.25	0.50	0.75	1.00	1.25	1.50	1.75	2.00
25	23.50	29.50	35.50	36.70	36.30	35.50	34.70	33.50	32.30
50	25.10	31.50	37.50	38.30	38.30	37.10	36.30	35.10	33.90
75	28.24	34.09	39.94	41.29	40.84	39.94	38.59	37.24	36.34
100	28.37	35.38	41.88	43.38	42.88	41.88	40.88	39.34	38.34
120	29.56	36.71	43.86	46.06	46.06	45.51	43.86	42.76	41.66
140	31.05	40.65	49.05	52.05	52.65	51.45	50.25	48.45	46.65

* Pressure in MPa and temperature in °C

Table 6.b Burst pressure varying with gradient temperature and thickness ratio (Case 3: winding angle 30°)

	Thickness Ratio									Temp.
Temp.	0.10	0.25	0.50	0.75	1.00	1.25	1.50	1.75	2.00	Difference
25-140	20.30	24.30	25.50	24.70	23.50	22.30	21.10	20.30	19.50	115
50-120	23.29	28.24	30.49	29.90	29.14	27.79	26.89	25.50	24.64	70
75-100	26.88	33.38	36.88	37.50	36.88	35.89	34.38	33.10	32.38	25
140-25	15.90	18.30	21.90	24.30	25.90	26.70	27.50	27.90	27.90	115
120-50	19.69	23.29	27.34	30.30	31.84	32.74	33.19	33.10	33.19	70
100-75	25.38	30.34	35.88	38.30	39.38	39.88	39.34	37.90	36.38	25
85-85	25.38	30.34	35.88	38.30	39.38	39.88	39.34	37.90	36.38	0

* Pressure in MPa and temperature in °C

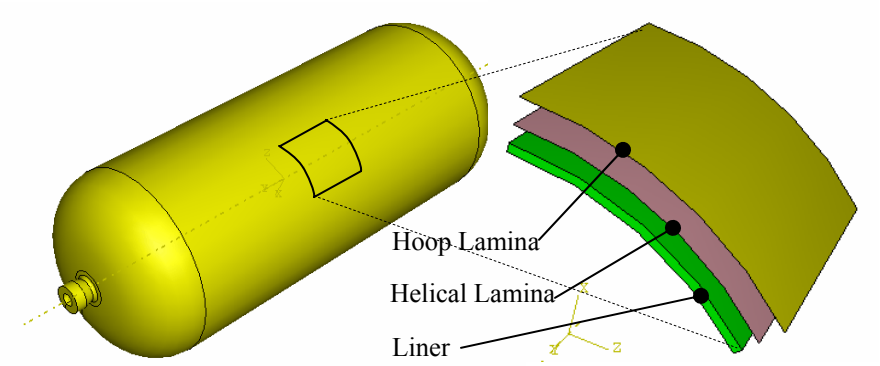

Figure 1 High pressure composite cylinder

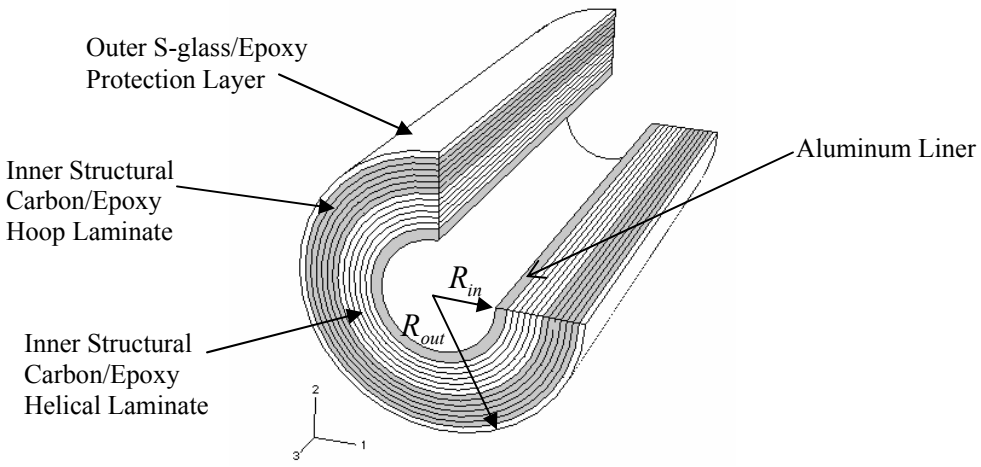

Figure 2 Cross-section of hydrogen storage cylinder

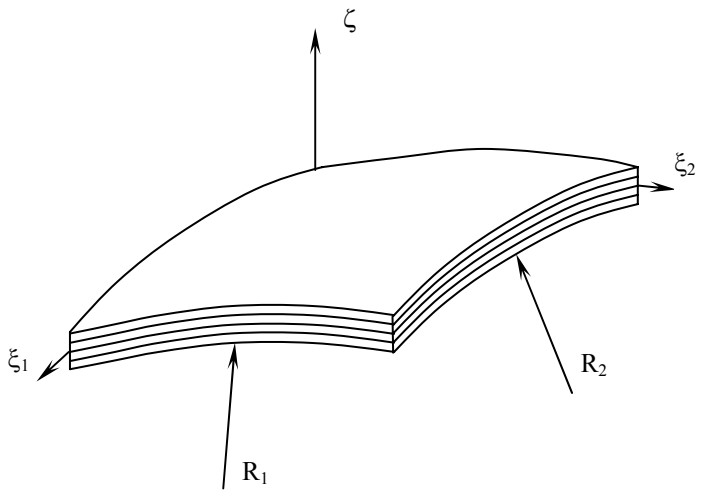

Figure 3 Doubly curved shell and coordinate system

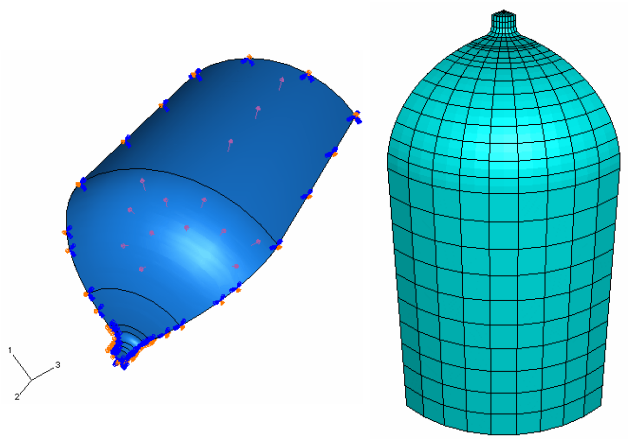

Figure 4 Finite element model of hydrogen storage cylinder

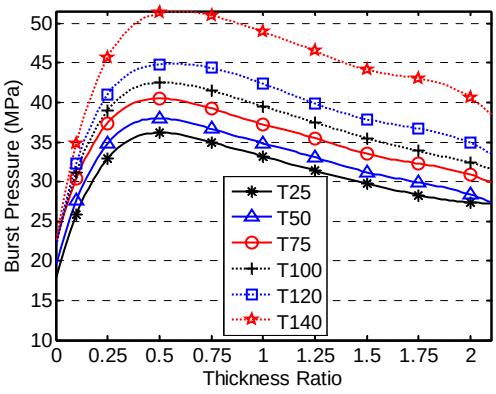

Figure 5 Uniform thermal loading (Case 1)

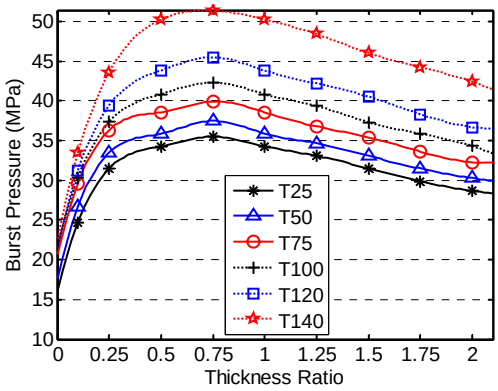

Figure 6 Uniform thermal loading (Case 2)

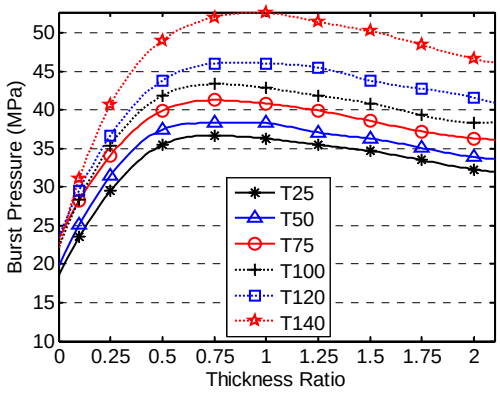

Figure 7 Uniform thermal loading (Case 3)

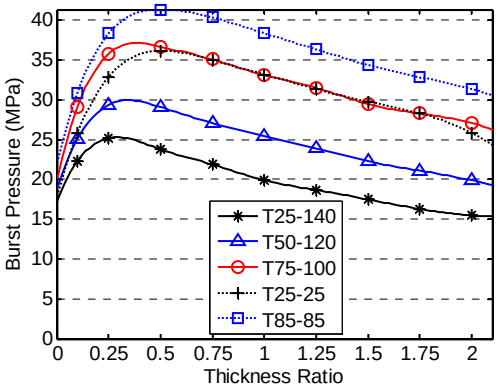

Figure 8 Gradient thermal loading with lower inner temperature (Case 1)

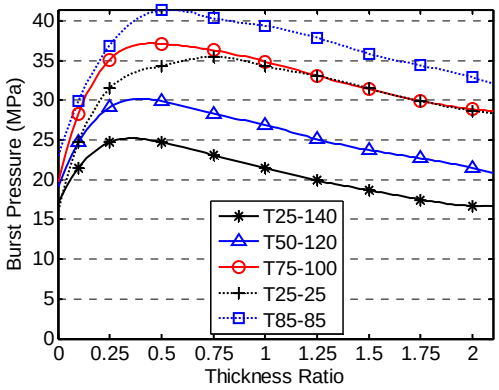

Figure 9 Gradient thermal loading with lower inner temperature (Case 2)

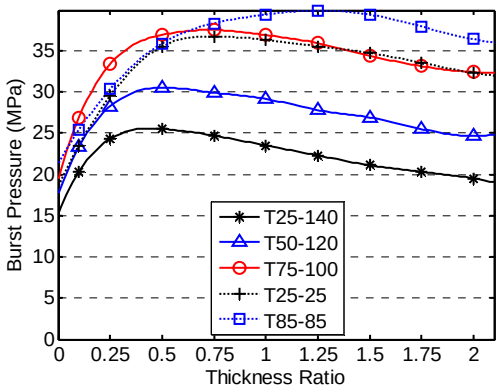

Figure 10 Gradient thermal loading with lower inner temperature (Case 3)

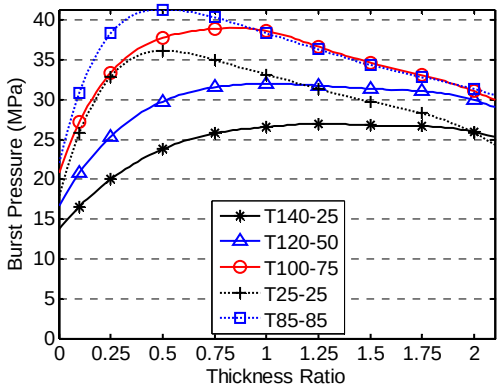

Figure 11 Gradient thermal loading with higher inner temperature (Case 1)

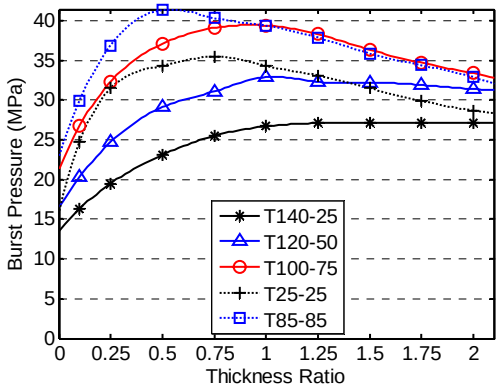

Figure 12 Gradient thermal loading with higher inner temperature (Case 2)

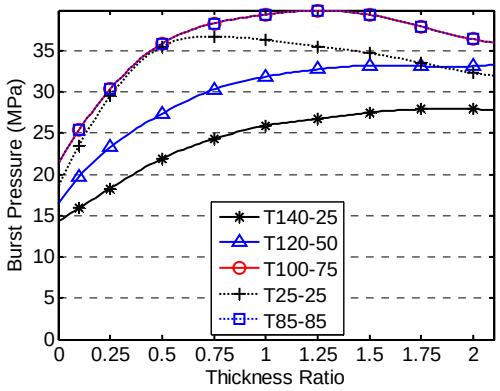

Figure 13 Gradient thermal loading with higher inner temperature (Case 3)

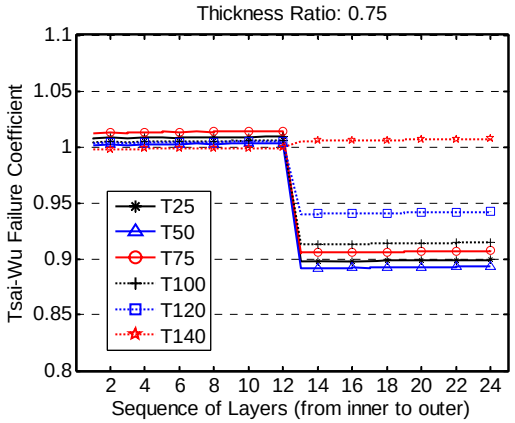

Figure 14 Failure evaluation (Tai-Wu theory) under uniform thermal loading (Case 2)

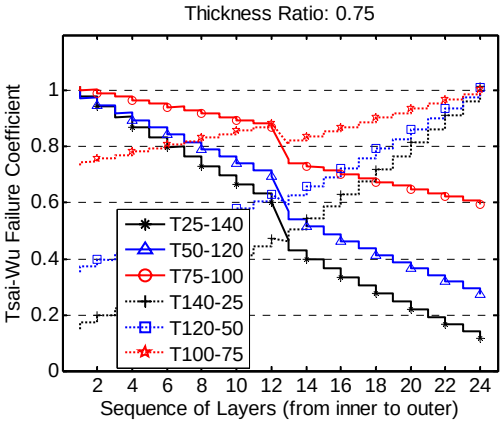

Figure 15 Failure evaluation (Tai-Wu theory) under non-uniform thermal loading (Case 2)